

## Research with High-Power Short-Wavelength Lasers

J. F. Holzhrichter, E. M. Campbell, J. D. Lindl, E. Storm

The development in the mid-1960's of lasers with high peak power made it possible to create states of matter in the laboratory that had previously existed only under astrophysical conditions or in nuclear explosions. In anticipation of the ability to create such conditions on large

required for many of the proposed applications. In these early experiments, much of the physics of high-intensity laser-matter interactions was examined (4). These experiments gave impetus to the technological proposals, but they also indicated that there was nonclassical or

**Summary.** Three high-temperature, high-density experiments were conducted recently with the 10-terawatt, short-wavelength Novette laser system at the Lawrence Livermore National Laboratory. The experiments demonstrated successful solutions to problems that arose during previous laser-plasma interaction experiments with long-wavelength (greater than 1 micrometer) lasers: (i) large-scale plasmas, with dimensions approaching those needed for high-gain inertial fusion targets, were produced in which potentially deleterious laser-plasma instabilities were collisionally damped; (ii) deuterium-tritium fuel was imploded to a density of 20 grams per cubic centimeter and a pressure of  $10^{10}$  atmospheres under the improved laser conditions, and compression conditions (preheating and pressure) were consistent with code calculations that predict efficient (high-gain) burn of a large thermonuclear fuel mass when driven with a large, short-wavelength laser; and (iii) soft x-rays were amplified by a factor of 700 by stimulated emission at 206 and 209 angstroms (62 electron volts) from selenium ions in a laser-generated plasma. These small, short-pulse x-ray sources are  $10^{10}$  to  $10^{11}$  times brighter than the most powerful x-ray generators and synchrotron sources available today. The plasma conditions for these experiments were made possible by advances in Nd:glass laser technology, in techniques to generate efficiently its short-wavelength harmonics at 0.53, 0.35, and 0.26 micrometers, and in diagnostic and computational modeling.

scales ( $\sim 1$  cm), a variety of technologies were proposed, including laser-driven thermonuclear implosions (1, 2) and x-ray lasers (3) (Fig. 1). Because high-quality laser light can be focused easily to dimensions less than 30  $\mu\text{m}$ , early lasers (delivering typically 1 J of energy in a nanosecond pulse) generated intensities in excess of  $10^{14}$   $\text{W cm}^{-2}$ . This intensity was sufficient to heat matter in the focal region to temperatures approaching 1 keV ( $10^7$  K), which are re-

anomalous behavior in the laser-plasma interaction (5). However, the small dimensions of the experiments ( $\sim 30$   $\mu\text{m}$ ) precluded tests of the key physical models.

By the early 1970's Nd:glass lasers operative at 1.06  $\mu\text{m}$  were being used in experiments at a few tens of joules in 0.1-nsec pulses. This output gave  $10^{11}$  W of power (0.1 TW) which, when focused to a spot size of about 100  $\mu\text{m}$ , provided a peak intensity of up to  $10^{15}$   $\text{W cm}^{-2}$ .

When the light from these systems was focused onto glass Microballoons that contained deuterium and tritium (DT) gas, fusion conditions were achieved. Neutrons generated by thermonuclear fusion were first reported at KMS Fusion (6) and soon thereafter at Lawrence Livermore National Laboratory, where their origin was confirmed (7), and elsewhere (8).

These experiments gave further impetus to proposals for inertial confinement fusion (ICF) and other high-temperature research. However, theoreticians noted (9) that, in the larger plasmas ( $\sim 1$  cm) necessary for full-scale demonstrations of these technologies, very nonthermal conditions (laser-plasma instability) could occur if the laser wavelength or the plasma were "too long." When laser-plasma experiments were conducted at 100 to 1000 J and with 0.1- to 0.5-nsec pulses, many targets showed energy partitioning into the suprathermal electron population exceeding 50 percent of the absorbed energy, levels of backscattered laser radiation exceeding 40 percent, and poor conversion of laser light into thermal x-rays. Early attempts to achieve high fuel compression and efficient thermonuclear neutron production from ICF targets with the Shiva laser at Livermore (1.06- $\mu\text{m}$  wavelength, 10-kJ pulse energy) (8) and with the Helios laser at Los Alamos (10.6  $\mu\text{m}$ , 10 kJ) (8) were not successful. Also, relatively straightforward physics measurements, such as shock-wave velocities and atomic physics spectral studies, were complicated because of very energetic plasma electrons. In spite of these difficulties, progress in understanding plasma scaling was made through the use of 1- $\mu\text{m}$  and 10- $\mu\text{m}$  lasers. Our colleagues at Livermore demonstrated DT fuel compression in an ICF target (10) that approached 20  $\text{g cm}^{-3}$  (100 times the density of liquid DT), although the target was complex and the compression conditions were not

The authors were technically responsible for the areas discussed in this article as follows: J. F. Holzhrichter, inertial fusion direction and laser research; E. M. Campbell, laser-plasma experiments and diagnostics; J. D. Lindl, theory and numerical modeling; and E. Storm, inertial confinement fusion experiments and direction. Their address is Lawrence Livermore National Laboratory, Livermore, California 94550.

suitable for efficient fusion. With the use of low-energy (1 to 100 J), short-wavelength laser light and improved simulation techniques, further progress was made in understanding the coupling between laser light and the plasma waves (8). It became clear that larger short-wavelength lasers ( $\lambda$ ,  $<1 \mu\text{m}$ ) were required for continued progress.

With the present generation of high-power, short-wavelength lasers (11), we can now produce energies in the range of 10 to 100 kJ at wavelengths of  $0.5 \mu\text{m}$  or shorter and with pulse durations of the order of  $10^{-9}$  second (Fig. 2). These laser systems, in conjunction with sophisticated diagnostic and computational capabilities, have made it possible to propose fusion and x-ray laser experiments at scales large enough to test many of their basic premises.

In addition to the detailed ICF and x-ray laser experiments described here, short-wavelength lasers are being used to make measurements in a variety of other scientific disciplines. Examples include the acceleration of metal foils (mass,  $10^{-6}$  g) at  $10^{16}$  cm sec $^{-1}$  ( $10^{13}$  g) to speeds near  $10^7$  cm sec $^{-1}$  (12), generation of shock pressures greater than 70 Mbar (13), and x-ray sources with brightnesses of more than  $10^{14}$  W cm $^{-2}$  sr $^{-1}$  (14) and with pulse durations from  $10^{-10}$  to  $10^{-8}$  second (15).

### Plasma Instabilities

The process by which laser light deposits energy in the target plasma determines the subsequent hydrodynamic motion, the atomic physics, and the energy transport. All these phenomena are strongly affected by the electron and ion energy distributions produced during the absorption process. This interaction at the high intensities required for many of the applications has been difficult to understand because numerous parametric instabilities and laser self-focusing can be strongly excited (9, 16, 17). In the extremely nonuniform plasmas typical of ICF applications, it has been particularly difficult to predict the thresholds for the onset of these collective plasma processes and their nonlinear saturation levels.

Laser energy couples to a plasma through several processes that can be grouped generally into two categories: collisional or collective. In one kind of collisional process, the plasma electrons, oscillating in the laser electric field, are scattered by the much heavier ions, thus converting the coherent laser energy into random (thermal) energy that is characteristically from 1 to 5 keV. This pro-

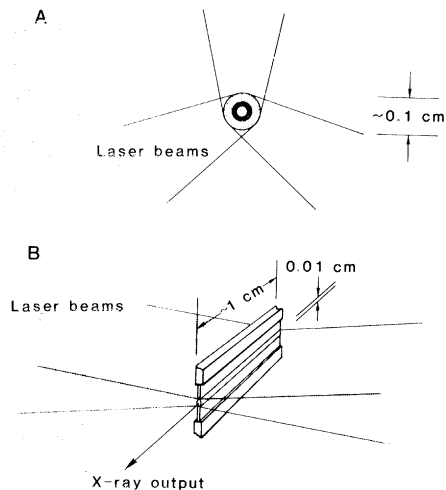


Fig. 1. (A) High-gain inertial confinement fusion target, composed of solid-density DT fuel contained in an ablator. (B) Soft x-ray laser target, composed of thin films of selenium or yttrium, are irradiated by line-focused laser beams. Dimensions are typical for present laser-target experiments.

cess, called inverse bremsstrahlung absorption, can be very efficient in absorbing laser light and is the desired coupling process for most applications.

In contrast, collective (or collisionless) absorption processes can lead to the generation of highly energetic electrons with typical energies in the range of 10 to greater than 100 keV. The physical mechanism underlying this type of coupling arises from the long-range nature of the Coulomb force, which allows plasmas to support both low- and high-frequency charged particle oscillations without collisional interaction. These plasma waves can be driven to high amplitudes by the high-intensity, rapidly varying electric field of the laser. The electric field associated with the high-frequency plasma density fluctuations can effectively accelerate (heat) electrons, particularly those that are traveling near the phase velocity of the plasma waves. However, reducing the laser intensity below  $10^{14}$  W cm $^{-2}$  (and thus reducing the driving electric field of the laser) to avoid instability generation reduces the pressure below the nominal 50 Mbar required to implode fusion capsules. The laser energy that can be delivered to the target before performance is affected by plasma instabilities depends on the laser wavelength, the size of the plasma, and the target average atomic number ( $\bar{Z}$ ).

The plasma instabilities that have a major role in laser-plasma coupling can be characterized by the various daughter waves into which the incident laser photons decay (17). The Raman instability is decay of the laser light into an electron-

plasma wave (or Langmuir wave) and a scattered photon, the  $2\omega_{pe}$  instability is decay into two plasma waves, and Brillouin scattering is decay into a scattered photon and an ion-acoustic wave. The electron-plasma waves resulting from the Raman and  $2\omega_{pe}$  instabilities are generally damped by accelerating electrons in the plasma. This collisionless (or Landau) damping can produce very energetic electrons because the phase velocity of the plasma waves is usually much greater than the electron thermal velocity. The traveling charge gradients caused by the electron-plasma waves can generate a longitudinal electric field strength as great as  $10^9$  Vcm $^{-1}$ , which accelerates slower electrons. The accelerated (suprathermal) electrons can penetrate and preheat the fuel pellet, increasing the entropy of the fuel and making energy-efficient compression more difficult. Although this mechanism of acceleration is detrimental to the fusion application, it is being considered as a means of particle acceleration in high-energy physics research (18).

Brillouin scattering, although not capable of producing suprathermal electrons, can also prevent effective laser-plasma coupling. It produces an ion-acoustic wave (the plasma analog of a sound wave) that has a low phase velocity and couples well to the plasma ions. Because of the low frequency of this wave compared with that of the incident laser wave ( $\omega_{ia}/\omega_0 < 10^{-3}$ ), little energy is transferred from the ion-acoustic wave to the plasma. However, the scattered Brillouin light wave can carry away most of the laser energy, seriously degrading the absorption efficiency of the target.

Short-wavelength laser light reduces the effects of these instabilities in several ways. First, the light interacts with the matter at higher densities because the maximum electron density ( $n_c$ ) to which the laser can penetrate in the plasma is given approximately by the empirical relation  $(10^{21}\lambda^{-2})$  cm $^{-3}$ , when  $\lambda$  is in micrometers ( $10^{-4}$  cm). At this density, the electron plasma frequency is equal to the laser frequency, and laser-light propagation stops. However, because short-wavelength light propagates to a higher plasma density, where the electron-ion collision rates are higher, more light is absorbed along the propagation path through inverse bremsstrahlung absorption. Another consequence of the propagation to regions of higher density is that the net growth rates of the unstable plasma waves are reduced because of increased electron-ion collision damping. A further benefit of short-wavelength operation is that the transverse

electron velocity, driven by the oscillating laser field, is reduced. This velocity is proportional to  $(I\lambda^2)^{1/2}$ , so that at constant intensity ( $I$ ) it drops as  $\lambda$  is decreased. Because the transverse velocity (current) is the forcing function for the plasma instabilities, the instability growth rate also drops. A final consequence is that, with constant absorbed intensity, the higher density plasma remains cooler so that plasma-wave phase velocities are somewhat lower and the energy of the accelerated suprathermal electrons is less. This results in less preheating for a given number of suprathermal electrons, since the penetration range of these hot electrons scales as  $E^{1.5-2.0}$ . Figure 3 summarizes the effectiveness of laser-plasma coupling with short-wavelength lasers.

Kruer (19) has provided a map of plasma instability thresholds that self-consistently includes the above arguments (Fig. 4). In this map the instability thresholds for a gold plasma ( $\bar{Z} \sim 30$  to 50) are plotted from the two variables that most often dominate the threshold alternatives, the plasma size relative to the laser wavelength ( $L/\lambda$ ) and  $I\lambda^2$ , which determines the transverse electron velocity. Similar maps are available for plasmas with other values of  $\bar{Z}$ , in which the collision frequency (proportional to  $\bar{Z}$ ) is different.

Figure 4 shows that plasmas formed under conditions far to the right of the instability threshold lines have a disproportionate number of suprathermal electrons. Plasmas formed to the left of these lines exhibit classical absorption and are largely thermal. The thresholds (left) are determined by plasma collisionality, and they can become independent of plasma size and rise vertically (top left). Computer simulations and theory show that in this regime, when the electron-ion collision frequency is comparable to the instability growth rate, the instabilities are effectively damped and cannot become efficient. This is the regime in which high-gain targets can operate. Thresholds to the lower right in Fig. 4 are dominated by the relatively small laser-plasma interaction length ( $L/\lambda$ ). This places a limit on the length in the plasma over which the laser and daughter waves resonantly interact and exchange energy. Thus plasma gradients, which limit the interaction length, provide another effective damping mechanism. Experiments conducted between 1979 and 1981 with 10- to 100-J lasers at 1.06, 0.53, and 0.35  $\mu\text{m}$  probed this region and demonstrated the efficiency of short-wavelength coupling to plasmas on small scales (4, 8).

## Large-Scale Plasmas

Recent experiments performed with the Novette laser at 0.53 and 0.26  $\mu\text{m}$  (and earlier experiments on the Shiva laser at 1.06  $\mu\text{m}$ ) have shown the sensitivity of the laser-plasma coupling to the above variables for plasma dimensions  $10^3$  laser wavelengths long (20). Thin films of CH (thickness, 6  $\mu\text{m}$ ;  $\bar{Z} \approx 3$ ) and gold (0.4  $\mu\text{m}$ ;  $\bar{Z} \approx 30$  to 50) were irradiated and expanded so that the density dropped below the critical density, leading to a long interaction length. In experiments in which plasma inhomogeneity and collisional thresholds were exceeded with light of 1.06- and 0.53- $\mu\text{m}$  wavelength on CH and gold targets (Fig. 4), stimulated Raman scattering efficiencies as great as 3 to 10 percent of the laser energy were observed. Even with 0.26- $\mu\text{m}$  light and the CH target, efficient scattering was observed. But in experiments with gold plasmas and 0.26- $\mu\text{m}$  light (Fig. 4) in which plasma instability thresholds due to inhomogeneity were exceeded but collisional damping was dominant, the Raman scattering efficiency was reduced to less than  $10^{-3}$  percent, and high-energy x-rays, the signature of hot electrons, were not measurable. Because of the high absorption and low density of hot electrons, these collisionally stabilized plasmas provide satisfactory operating conditions for ICF implosions.

The demonstration of collisional stabilization is important because high-gain

targets driven with multimegajoule lasers will have plasmas for which  $L/\lambda$  is approximately  $10^4$ . In Fig. 4 the expected operating regime is located somewhat above the instability thresholds. Numerical simulations and these experiments indicate that, even though thresholds may be exceeded severalfold, the fraction of plasma hot electrons will be acceptably low (<5 percent) with laser wavelengths between 0.26 and 0.53  $\mu\text{m}$ . A major objective of laser-plasma experiments with the Nova laser is to verify that collisional stabilization provides the expected satisfactory plasma conditions for high-gain target performance.

## The Nd:Glass Laser

The rapid development of the harmonically converted Nd:glass laser system was motivated by the need for large-scale experiments and by the poor plasma conditions obtained with 1.06- and 10.6- $\mu\text{m}$  light. To date, almost all short-wavelength laser-plasma interaction studies have been conducted with the Nd system. However, the krypton fluoride laser, with output at 0.249  $\mu\text{m}$ , and the harmonically converted atomic iodine laser, with outputs at 1.3, 0.65, 0.44, and 0.32  $\mu\text{m}$ , can also be used and are being developed at several laboratories (4, 21, 22).

In the early 1970's, the Nd:glass laser was chosen as the major research tool for laser-plasma interaction research at



Fig. 2. The Novette laser, a harmonically converted Nd:glass laser that generated 9 kJ of 0.53- $\mu\text{m}$  light and 1.5 kJ of 0.26- $\mu\text{m}$  light for short-wavelength laser-plasma experiments. In August 1984, its two beams were removed and installed as two of the ten beams in the Nova laser, which was completed in December 1984 and is now being activated.

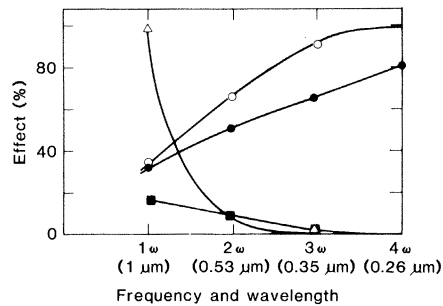
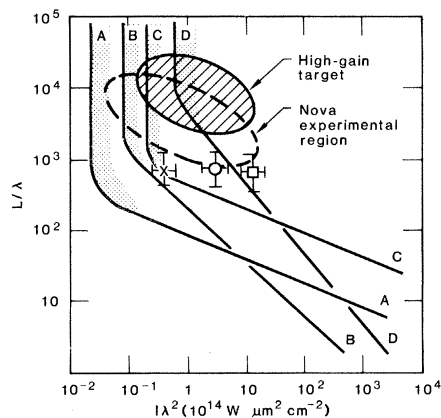


Fig. 3 (left). Laser-plasma coupling with short-wavelength lasers. The coupling to gold disks at intensities of  $3 \times 10^{14} \text{ W cm}^{-2}$  (500-psec pulses) improves as the laser wavelength is shortened. The signatures of plasma instabilities—energetic x-rays and scattered laser light—drop sharply. Symbols: ( $\Delta$ ) hot x-ray propagation, ( $\circ$ ) absorption, ( $\bullet$ ) x-ray conversion, and ( $\blacksquare$ ) backscatter. Fig. 4 (right). Laser-plasma interaction regimes for collisional and collective absorption processes, showing conditions for 0.26- $\mu\text{m}$  (X), 0.53- $\mu\text{m}$  ( $\circ$ ), and 1.06- $\mu\text{m}$  ( $\square$ ) laser plasma experiments on gold plasmas with scale lengths ( $L/\lambda$ ) of 1000. Thresholds are shown for two-plasmon decay (A), absolute Raman (B), Brillouin (C), and convective Raman (D) instabilities. Absorption occurs primarily by collisions (when the experimental conditions are to the left of the lines) and progressively more strongly by instabilities (when the experimental conditions move into the stippled region to the right of the lines). The experiment noted by X was in a collisionally stabilized region, in which less than  $10^{-3}$  percent scattered Raman light and no hot electrons were observed.



er more than 50 percent of the laser's 1.05- $\mu\text{m}$  energy to a target at 0.53  $\mu\text{m}$  (32). By using a second crystal after the first crystal, it is also possible to convert efficiently the fundamental 1.05- $\mu\text{m}$  radiation to the third or fourth harmonic at 0.35  $\mu\text{m}$  (up to 80 percent) (33) or 0.26  $\mu\text{m}$  (up to 50 percent) (34), respectively. For 0.26- $\mu\text{m}$  experiments, 1.5 kJ of light in a 1.0-nsec pulse was delivered to targets from one of the Novette laser chains. This energy was damage-limited not conversion-limited.

### Inertial Confinement Fusion

For most ICF applications, such as electricity production, high gains (greater than 100) are needed. High-gain ICF fusion occurs when 2 to 10 mg of DT fuel is compressed to a density exceeding  $200 \text{ g cm}^{-3}$  (electron and ion densities exceeding  $5 \times 10^{25} \text{ cm}^{-3}$ ) and when the thermonuclear burn of the fuel is initiated in a high-temperature ( $T_{\text{ion}} \sim 3$  to 5 keV) central hot spot (2, 35, 36). (Energy gain in ICF is defined as the ratio of the thermonuclear energy produced to the input laser energy.) To assemble the fuel in such a state, one must apply a precisely time-programmed ( $\sim 10$  nsec long) pressure pulse exceeding  $5 \times 10^7$  atmospheres (50 Mbar) at peak. Little preheating of the fusion fuel can be tolerated. For initial experiments, to achieve fusion gain approaching 100, we expect that 5 to 10 MJ of short-wavelength laser energy ( $\lambda < 0.5 \mu\text{m}$ ) is required. Target gains exceeding 100 with lower input energy are anticipated as technology and our understanding of the physics progress (37). By using the 0.53- $\mu\text{m}$  output from the Novette laser, we ablatively imploded DT fusion fuel to densities of  $20 \text{ g cm}^{-3}$ , or 100 times the density of solid DT fuel (38). The compression conditions achieved in these experiments (described below), together with improved targets and laser pulse shaping, will be used in upcoming experiments on the Nova laser to obtain fuel density approaching that needed (1000 times the density of liquid DT, or  $200 \text{ g cm}^{-3}$ ) for high-gain implosions. In addition, we expect that these compression conditions can be extended to targets designed for use with future multimegajoule laser drivers.

There are two laser-driven ICF techniques for generating the required pressures for compression and ignition: direct drive (2, 39), in which electrons transport the laser energy to the ablation surface, and indirect drive, in which x-rays transport the energy to the ablation

Livermore (8, 23). This choice was based on the system's versatility, scaling to high power levels, and the potential for harmonic conversion of its fundamental 1.06- $\mu\text{m}$  wavelength to shorter wavelengths. These features have been used to develop the laser we use today and result in easy variation of pulse duration and shape, high optical-damage thresholds leading to moderately compact systems, conveniently available beam diagnostics with film, silicon detectors, or vidicons, and straightforward size scalability to roughly 100 kJ through increased beam area or multiple beams. A variety of efficient harmonic conversion techniques invented for this system is used routinely to produce laser energy for experiments at 0.53, 0.35, and 0.26  $\mu\text{m}$ . The Nd:glass laser in its present form has not been considered for high-repetition rate ( $\sim 5$  Hz), high-efficiency ( $>10$  percent) applications such as pure-fusion reactor drivers. However, extensions of this technology that use crystalline solid-state laser media (24), as well as gas-laser (25), heavy-ion (26), and light-ion (27) technologies, are being investigated for this and other applications.

The development of the Nd:glass laser for fusion applications progressed rapidly from very simple oscillator-amplifier systems to more powerful systems producing a few tens of joules in 0.1 nsec by the early 1970's. These small systems were limited in their output by a nonlinear self-focusing (filamentation) instability of the laser beam (28). Subsequent improvements in our understanding of

high-intensity beam propagation led to the use of multiple-imaging spatial filters (29) to control the growth of this instability. As a result, longer, larger diameter amplifier chains were constructed before the beam reached the self-focusing thresholds, and higher output power from each aperture was obtained. New laser host glasses (30) were developed that have a lower nonlinear index of refraction, a higher cross section, and a slightly shorter wavelength (1.05  $\mu\text{m}$ ). Together with new optical-surface preparations and coatings (31), the new glasses permitted further increases in output power from each aperture. These and other advances led to designs for the Novette and Nova lasers (11), which produce more than 10 TW of focusable power per beam in 100 psec, or more than 12 kJ per beam in 5 nsec at 1.05  $\mu\text{m}$ .

### Harmonic Conversion

Efficient harmonic conversion to shorter wavelengths from these lasers is feasible because the phase uniformity of high-power beams from modern lasers is of high quality and the power density is high ( $10^9 \text{ W cm}^{-2}$ ). For example, with a properly oriented 1.8-cm thick crystal of potassium dihydrogen phosphate (KDP), we can convert a 1.05- $\mu\text{m}$  laser beam at  $2 \text{ GW cm}^{-2}$  to the second harmonic at 0.53  $\mu\text{m}$  with up to 80 percent efficiency. When losses of the optical components (lenses, diagnostics, blast shields, and the like) of a fusion laser beam line are taken into account, it is possible to deliv-

surface. Critical issues that are determining the viability of both approaches are symmetry, stability, fuel preheating, and implosion efficiency (8, 40). In the direct-drive approach, the energy of the laser driver is focused and absorbed at the surface of a spherical ablator surrounding the fuel container. Heating and subsequent mass ablation generates the pressure that drives the implosion. The ablation pressure ( $P_a$ ) that can be generated depends strongly on the absorbed laser intensity ( $I$ ), and theory and experiment have shown that  $P_a \propto I^{0.5-0.6}$  (41).

In the indirect-drive approach, which is the principal focus of ICF research at Livermore, the laser light is converted to soft thermal x-rays contained in a high-atomic number "hohlraum." The soft x-rays in the hohlraum drive the target capsule. If submicrometer light is used (14), efficient conversion of laser light into thermal x-rays can occur. An advantage of this approach is that it can produce a highly symmetric implosion with a relatively poor laser focal distribution. It also does not require uniformly arrayed laser beams, which is an advantage for ICF reactor designs.

## Compression

The improved coupling of 0.53- $\mu\text{m}$  laser light from Novette has made possible the ablative implosion of fusion capsules to substantially higher densities than were obtained on Shiva for similar capsules at similar energies. For determining the compression of the imploded target, the areal density (the product of density and thickness,  $\rho\Delta r$ ) of the compressed fuel container was measured (38). The container is referred to as the capsule pusher because of its role in the compression processes. When the target is driven to high density, both the pusher areal density and the fuel density increase significantly. This is in contrast to strongly preheated targets, such as the exploding pusher targets first used in ICF demonstrations (6, 42) in which the pusher areal density remained relatively unchanged. In our high-density implosions, 14-MeV neutrons were produced by the fusion of DT near the time of peak target compression. Activation of the pusher material by these neutrons (43) is proportional to the pusher areal density at that time (we infer the fuel density by comparing the measured pusher activation with the results of simple analytical models and hydrodynamic code calculations that self-consistently described both the pusher and fuel density). As shown in Fig. 5, we measured increases

in the pusher areal density from its initial value by factors as great as 60 to 80 when using 0.53- $\mu\text{m}$  irradiation. This compression of the pusher is three to five times greater than in similar 1.06- $\mu\text{m}$  experiments on Shiva and implies compressed fuel densities in excess of  $20 \text{ g cm}^{-3}$ . By using 30 to 50 kJ of 0.35- $\mu\text{m}$  light from the Nova laser to extend these results, we should be able to achieve the DT fuel densities required for high-gain target operation.

## X-ray Lasers

The prospect of generating laser action at x-ray wavelengths has been discussed since the invention of the laser (44). Although many potential schemes (45) have been identified that could lead to gain at wavelengths near  $100 \text{ \AA}$ , until recently many difficulties prevented unambiguous confirmation. We observed (45) stimulated emission at 206 and 209  $\text{\AA}$  in the soft x-ray region from thin-foil selenium targets. The experiments utilized a 2-TW, 450-psec pulse from the Novette laser to irradiate foils up to 2.2 cm long at a power density of  $5 \times 10^{13} \text{ W cm}^{-2}$  with 0.53- $\mu\text{m}$  light.

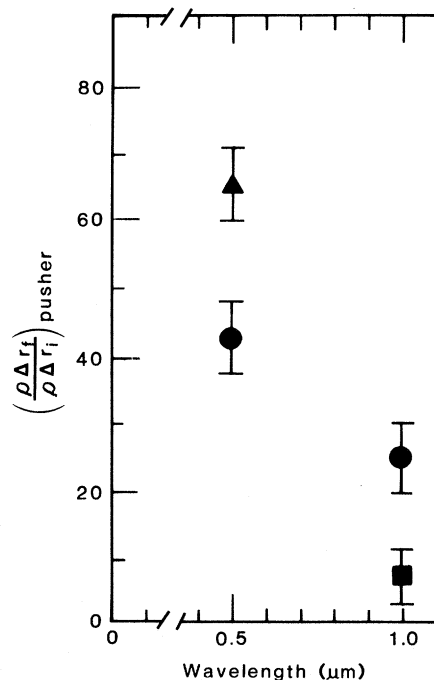


Fig. 5. Direct measurement of the areal density of the DT fuel container (pusher) by means of neutron-activation techniques, showing the increase in pusher compression using virtually identical irradiation conditions. From this increase, we infer that the compression is ablative and that the density of the DT fuel reached greater than 100 times that of liquid DT. Symbols: (●) results from identical hohlraum targets; (▲) and (■) pusher compressions from slightly different targets.

One of the most demanding requirements was to find and produce a medium with a sufficient gain-length product to produce measurable line enhancement on a single pass through the plasma. At present, there are no suitable cavity configurations to provide multiple passes through the gain medium (46). Other physical constraints arose because the small signal gain (for fixed Einstein A coefficient) scales as  $\lambda^3 T_i^{-1/2}$  ( $T_i$ , irradiation temperature) because suitable soft x-ray transitions have short lifetimes ( $\geq 5 \times 10^{-11}$  second) and because the efficiency of channeling pump energy into the upper laser state is inherently low (47). These considerations lead to the requirement that the pump power exceed  $10^{13} \text{ W cm}^{-2}$ . For there to be net laser gain, it was also necessary that the ionic density be large enough, that the propagation path be sufficiently uniform to prevent refraction of the beam out of the gain medium, and that absorption losses from other ionic transitions be absent. These conditions were satisfied by using 0.53- $\mu\text{m}$  light on an exploding-foil target made from selenium (thickness, 750  $\text{\AA}$ ) on a 1500- $\text{\AA}$  Formvar backing (45). Finally, temporally and spectrally resolved diagnostics were required to differentiate gain from the intense emission of neighboring transitions that occur during the laser pulse and in the afterglow of the relaxing plasma (48).

The gain was produced in these experiments by electron collisional excitation of neon-like ions. It has long been recognized that large differences in the radiative decay rates of the  $2p^5 3p$  and  $2p^5 3s$  states in neon-like ions can lead to a population inversion between these states in an optically thin plasma (49). Calculations based on isoelectronic scaling of the neon-like configuration in ions of higher Z showed that gain at the extreme ultraviolet and soft x-ray wavelengths was possible with a sufficiently high pumping rate (47). The required pumping rate was achieved by bringing two opposing Novette laser beams to a common line focus on the target. The focusing was done with a combination of a cylindrical and a spherical lens.

Amplification of the neon-like  $3p^5 3p$  to  $3p^5 3s$  emission in selenium can be readily seen in the on-axis trace in Fig. 6, which shows the x-ray spectrum under maximum gain conditions along the plasma axis. The lines at 206 and 209  $\text{\AA}$  dominate the spectrum. The off-axis spectrum in Fig. 6 was recorded on the same shot, transverse to the plasma axis, and it recorded energy from the total radiating plasma volume. The lines at 206 and 209  $\text{\AA}$  were not observed be-

cause they were not amplified in the short transverse direction. The time-resolved measurement (Fig. 6, inset) was made with an absolutely calibrated spectrometer. It and similar measurements indicated a lower bound of 35 to 50 keV for the brightness temperature of these amplified lines. This temperature is consistent only with x-ray gain, not with thermal plasma processes associated with the plasma-electron temperature of less than 1 keV. The intensities of nearby lines, which are not amplified, correspond to equivalent temperatures of only about 0.1 keV. A small-signal gain coefficient of about  $6 \text{ cm}^{-1}$  was inferred for both lines from experiments in which the plasma length was varied from 0.1 to 1.2 cm. Similar experiments with  $\text{Y}^{29+}$  produced equivalent brightness temperatures of about 10 keV at  $154 \text{ \AA}$ , demonstrating isoelectronic scaling of the neon-like transitions to shorter wavelengths.

The peak output spectral brightness obtained from this laser system is

$2 \times 10^{11} \text{ W cm}^{-2} \text{ \AA}^{-1} \text{ sr}^{-1}$ . This is  $10^{10}$  to  $10^{11}$  times greater than today's most powerful x-ray generators and synchrotron sources (50). However, x-ray lasers are presently one-shot, short-pulse devices that need a great deal of additional development before they become useful laboratory x-ray sources.

### Conclusions

A wide variety of experiments have become possible with the development of multiterawatt, short-wavelength lasers. The Nova laser, providing 30- to 50-TW output at 0.53 and 0.35  $\mu\text{m}$ , will be used to extend laser-plasma studies to plasma scales approaching those needed for high-gain targets. These experiments should confirm our theoretical and experimental understanding of the laser-plasma coupling and of the implosion physics of the capsules required for high-gain operation. We expect to extend x-

ray laser performance to shorter wavelengths, higher power, and increased spatial coherence, and we will conduct a variety of shock-wave, atomic-physics, and hydrodynamic experiments.

### References and Notes

1. S. Colgate, R. E. Kidder, J. H. Nuckolls, R. F. Zabawski, E. Teller, unpublished calculations; N. G. Basov and O. N. Krokhin, in *Proc. Quantum Electron. Int. Conf.* 3, N. Bloembergen and P. Grivet, Eds. (Columbia Univ. Press, New York, 1964), vol. 2, pp. 1373-1963.
2. J. H. Nuckolls, L. L. Wood, A. R. Thiessen, G. B. Zimmerman, *Nature (London)* **239**, 139 (1972).
3. L. I. Gudzenko and L. A. Shelepin, *Sov. Phys. JETP* **18**, 998 (1964); R. W. Waynant and R. C. Elton, *Proc. IEEE* **64**, 1059 (1976).
4. H. J. Schwarz and H. Hora, Eds., *Laser Interaction and Related Plasma Phenomena* (Plenum, New York, 1971-84), vols. 1-6.
5. J. W. Shearer et al., *Phys. Rev. A* **6**, 764 (1972).
6. G. Charatis et al., *Plasma Phys. Controlled Nucl. Fusion Res.* **2**, 317 (1974).
7. K. R. Manes, H. G. Ahlstrom, R. A. Haas, J. F. Holzrichter, *J. Opt. Soc. Am.* **67**, 717 (1977).
8. For detailed descriptions of laser systems and laser-plasma investigations, see the annual reports from the following laboratories: CEA Limeil, France; KMS Fusion, Inc., Ann Arbor, Mich.; Naval Research Laboratory, Washington, D.C.; Osaka University, Osaka, Japan; Sandia Laboratories, Albuquerque, N.M.; Lebedev Institute, Moscow, U.S.S.R.; Max-Planck Institute for Plasma Physics, Garching, West Germany; Rutherford Laboratory, Didcot, England; Lawrence Livermore National Laboratory, Livermore, Calif.; Los Alamos Scientific Laboratory, Los Alamos, N.M.; and University of Rochester Laboratory for Laser Energetics, Rochester, N.Y.
9. C. S. Liu, M. N. Rosenbluth, R. B. White, *Phys. Fluids* **17**, 1211 (1974); P. K. Kaw, W. L. Kruer, C. S. Liu, K. Nishikawa, *Adv. Plasma Phys.* **6**, 237 (1976).
10. See Lawrence Livermore Natl. Lab. Laser Prog. Rep. UCRL-50021-80, p. 7-1 (1980).
11. K. Manes et al., Lawrence Livermore Natl. Lab. Rev. UCRL-90054-1 (1984); W. W. Simmons et al., "Nova," in *Proc. Symp. Eng. Prob. Fusion Res.* 9 (IEEE publication 81CH1715-2 NPS), vol. 2, pp. 1221-1273.
12. S. P. Obenschain et al., *Phys. Rev. Lett.* **50**, 44 (1983).
13. B. Yaakobi et al., *Opt. Commun.* **39**, 175 (1981); F. Cottet, J. P. Romain, R. Fabbro, B. Faral, *Phys. Rev. Lett.* **52**, 1884 (1984).
14. R. L. Kauffman et al., *Bull. Am. Phys. Soc.* **29**, 1183 (1984).
15. L. L. Endelman, Ed., *Soc. Photogr. Instrum. Eng.* **348**, 1 (1982).
16. C. E. Max, *Physics of Laser Fusion* (Lawrence Livermore National Laboratory, Livermore, Calif., 1981), vol. 1. Available as Lawrence Livermore Natl. Lab. Rep. UCRL-53107.
17. D. W. Forslund, J. M. Kindel, E. L. Lindman, *Phys. Fluids* **18**, 1002 (1975); D. W. Phillion, E. M. Campbell, K. G. Estabrook, G. E. Phillips, F. Ze, *Phys. Rev. Lett.* **49**, 1405 (1982); K. Estabrook, W. L. Kruer, B. F. Lasinski, *ibid.* **45**, 1399 (1980).
18. C. Joshi et al., *Nature (London)* **311**, 525 (1984).
19. C. E. Max et al., *Laser Interaction and Related Plasma Phenomena*, H. J. Schwarz and H. Hora, Eds. (Plenum, New York, 1984), vol. 6, p. 507.
20. R. E. Turner, et al., *Phys. Rev. Lett.* **54**, 189 (1985).
21. E. T. Salesky and W. D. Kimura, Los Alamos Natl. Lab. Rep. LA-UR-84-4040; *ibid.* LA-UR-84-4038; *ibid.* LA-UR-84-4039.
22. G. Brederlow, K. J. Witte, E. Fill, K. Hohla, R. Volk, *IEEE J. Quantum Electron.* **QE-12**, 152 (1976).
23. J. F. Holzrichter et al., *J. Fusion Energy* **2**, 5 (1982). Available as Lawrence Livermore Natl. Lab. Rep. UCRL-52868-1. See also *Laser Prog. Annu. Repts. UCRL-50021-73 to UCRL-50021-84*.
24. J. L. Emmett, W. F. Krupke, J. B. Trenholme, *Physics of Laser Fusion* (Lawrence Livermore National Laboratory, Livermore, Calif., 1982), vol. 4. Available as Lawrence Livermore Natl. Lab. Rep. UCRL-53344.
25. C. K. Rhodes, Ed., *Topics in Applied Physics* (Springer, New York, ed. 2, 1984), vol. 30.
26. *Heavy Ion Accelerators and Their Applications*

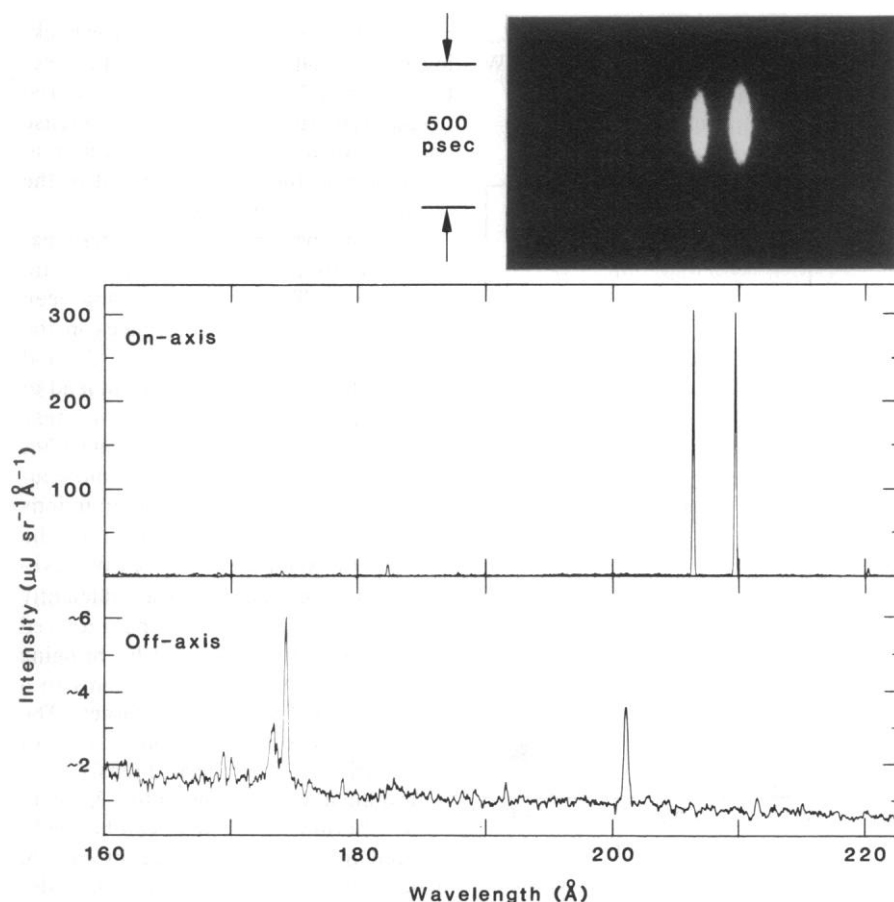


Fig. 6. On- and off-axis film data from a time-gated grazing-incidence spectrograph and x-ray streak camera. The traced data represent photons accumulated from the beginning of radiative output until approximately 500 psec after the peak intensity of the pump laser pulse. The on-axis data show the two strongest lines at maximum gain from a 2.2-cm long selenium laser compared to background. (Inset) The same lines time-resolved. The off-axis traced data show the spectral output from the entire plasma, viewed at an angle of  $73^\circ$  to the laser gain axis; laser lines are so weak and spontaneous that they are not visible. The absolute intensity scale for the off-axis data is approximately 50 times more sensitive than for the on-axis data, as evidenced by the relative intensities of the spontaneous, sodium-like lines at 174 and 200  $\text{\AA}$ .

to *Inertial Fusion* (Institute for Nuclear Study, Tokyo, Japan, 1984).

27. J. P. Van Devender *et al.*, *Laser Particle Beams* **3**, 93 (1985).
28. V. I. Bespalov and V. I. Talanov, *JETP Lett.* **3**, 307 (1966).
29. W. W. Simmons *et al.*, *IEEE J. Quantum Electron.* *QE-II*, 31D (1975); A. Bettinger, C. Charles, J. Osmalin, J. G. Giraud, *Opt. Commun.* **18**, 176 (1976); J. T. Hunt, J. A. Glaze, W. W. Simmons, P. A. Renard, *Appl. Opt.* **17**, 2053 (1978).
30. N. L. Boling, A. J. Glass, A. Owyong, *IEEE J. Quantum Electron.* *QE-14*, 601 (1978); S. E. Stokowski, R. A. Saroyan, M. J. Weber, *Nd-Doped Laser Glass: Spectroscopic and Physical Properties* (Lawrence Livermore National Laboratory, Livermore, Calif., 1981). Available as *Lawrence Livermore Natl. Lab. Spec. Pub. M-95-Rev. 2* (1981).
31. *Laser-Induced Damage in Optical Materials* (Special Publications, National Bureau of Standards, Washington, D.C., 1976 to 1984).
32. M. A. Summers *et al.*, *Lawrence Livermore Natl. Lab. Rep. Conf-811040* (1982), chap. 8, pp. 78-88; D. Eimerl, *Lawrence Livermore Natl. Labs. Energy Technol. Rev.* (August 1982).
33. W. Seka *et al.*, *Opt. Commun.* **34**, 469 (1980); R.

- S. Craxton, *ibid.*, p. 474; G. J. Linford *et al.*, *Appl. Opt.* **21**, 3633 (1982); *ibid.* **22**, 1957 (1983).
34. T. Reintges and R. C. Eckart, *Appl. Phys. Lett.* **30**, 91 (1977).
35. J. L. Emmett, J. H. Nuckolls, L. L. Wood, *Sci. Am.* **230**, 24 (June 1974).
36. J. Meyer-Ter-Vehn, *Nucl. Fusion* **22**, 561 (1982).
37. J. H. Nuckolls, *Phys. Today* **35**, 24 (September 1982).
38. F. Ze *et al.*, *Lawrence Livermore Natl. Lab. Rep. UCRL-91087* (1984).
39. S. E. Bodner, *J. Fusion Energy* **1**, 221 (1981).
40. C. E. Max, J. D. Lindl, W. C. Mead, *Nucl. Fusion* **23**, 131 (1983).
41. T. J. Goldsack *et al.*, *Opt. Commun.* **42**, 55 (1982).
42. E. K. Storm *et al.*, *Lawrence Livermore Natl. Lab. Laser Prog. Annu. Rep. UCRL-50021-76*, 5 (1977); *ibid. UCRL 50021-77* (2), 6 (1978).
43. E. M. Campbell *et al.*, *J. Appl. Phys.* **51**, 6062 (1980); *ibid.*, p. 6065.
44. A. L. Schawlow and C. H. Townes, *Phys. Rev.* **112**, 1940 (1958).
45. D. L. Matthews *et al.*, *Phys. Rev. Lett.* **54**, 110 (1985); M. D. Rosen *et al.*, *ibid.*, p. 106.
46. In recent work, x-ray mirrors with greater than 50 percent normal-incidence reflectivity near 200 Å have been made [T. W. Barbee, Jr., *AIP*

- Conf. Proc.* **119**, 311 (1984); E. S. Spiller, *ibid.*, p. 312].
47. P. L. Hagelstein, *Plasma Phys.* **25**, 1345 (1983).
48. N. M. Ceglio, *Rev. Sci. Instrum.*, in press.
49. A. V. Vinogradov *et al.*, *Sov. J. Quantum Electron.* **7**, 32 (1977); P. L. Hagelstein, *Lawrence Livermore Natl. Lab. Rep. UCRL-53100* (1981); A. V. Vinogradov and V. Shlyaptsev, *Sov. J. Quantum Electron.* **13**, 1511 (1983).
50. C. K. Rhodes, *Report on VUV and X-Ray Sources of Atomic and Molecular Science Workshop* (National Academy Press, Washington, D.C., in press).
51. We thank our colleagues in the Lawrence Livermore National Laboratory ICF Program and elsewhere who led the projects reviewed in this article: L. Coleman started the experimental and diagnostic program on Novette; I. Stowers and W. Hatcher led the teams who produced the targets; K. Manes, R. Speck, and G. Suski led the Novette effort; P. Drake, R. Turner, Y. Kauffman, D. Bach, K. Estabrook, and B. Lainski led the plasma physics experiments; F. Ze and S. Lane led the implosion experiments; and D. Matthews, M. Rosen, P. Hagelstein, N. Ceglio, and M. Eckhart led the x-ray laser effort. Supported by Lawrence Livermore National Laboratory (contract W-7405-ENG-48) under the auspices of the Department of Energy.

## Defining Lipid Transport Pathways in Animal Cells

Richard E. Pagano and Richard G. Sleight

Most of the enzymes responsible for lipid biosynthesis in animal cells reside on the rough and smooth endoplasmic reticulum (1); yet lipids are found in all the membrane systems of the cell, often with different intracellular organelles having different lipid compositions (2).

whose assembly into membranes, turnover, and secretion is one of the most actively studied areas in cell biology (4).

Our laboratory has developed an approach for studying lipid transport by means of fluorescent lipid derivatives that appear to behave as analogs of their

---

**Summary.** A new technique for studying the metabolism and intracellular transport of lipid molecules in living cells based on the use of fluorescent lipid analogs is described. The cellular processing of various intermediates (phosphatidic acid and ceramide) and end products (phosphatidylcholine and phosphatidylethanolamine) in lipid biosynthesis is reviewed and a working model for compartmentalization during lipid biosynthesis is presented.

---

Furthermore, some membranes exhibit an asymmetric distribution of lipids across the bilayer (3). Thus, a major problem in the cell biology of lipids is understanding how newly synthesized lipids are sorted into various intracellular compartments, and how these molecules are translocated or targeted to various destinations inside (or outside) the cell. This general problem is directly analogous to the study of cellular proteins

natural counterparts. With this methodology, it is now possible to examine the movements of fluorescent lipid molecules in the living cell by high-resolution fluorescence microscopy and correlate these data with the results of classical biochemical investigations. In this article we summarize recent findings obtained with this new technology and highlight possible future applications in cell biology.

### Incubation of Fluorescent

#### Lipids with Cells

Figure 1 shows the molecular structures of the three classes of fluorescent lipids we have used in our studies. The acyl chain-labeled lipids have high rates of spontaneous transfer in vitro (Table 1). For liposomes, this transfer occurs by dissociation of lipid monomers from one membrane, convection through the aqueous phase, and association with another membrane (5, 6). This property permits us to readily integrate the fluorescent lipids into cellular membranes from exogenous sources.

Our strategy for examining the intracellular metabolism and translocation of fluorescent lipid analogs is to first incubate cells at 2°C with liposomes containing both an acyl chain-labeled C<sub>6</sub>-NBD-lipid (7) and a nonexchangeable lipid [such as rhodamine-labeled phosphatidylethanolamine (*N*-Rh-PE) (8, 9)]. During this incubation, large amounts of the acyl chain-labeled analog but only small amounts of the nonexchangeable marker become associated with cells, suggesting that most (typically 90 to 99 percent) of the NBD-lipid is transferred to the cells by a spontaneous diffusion process. The cells are then washed and examined by fluorescence microscopy, or the lipids are extracted and analyzed by conventional analytical procedures. The cells can also be washed after the liposome incubation and then warmed to various temperatures prior to analysis.

---

Richard E. Pagano is a staff member and Richard G. Sleight is a postdoctoral fellow at the Department of Embryology, Carnegie Institution of Washington, Baltimore, Maryland 21210.